

Event-Triggered Islanding in Inverter-Based Grids

Ioannis Zografopoulos, *Graduate Student Member, IEEE*, Charalambos Konstantinou, *Senior Member, IEEE*

Abstract—The decentralization of modern power systems challenges the hierarchical structure of the electric grid and requires the implementation of automated schemes that can overcome adverse conditions. This work proposes an adaptive isolation methodology that can segregate a grid topology in autonomous islands that maintain stable and economic operation in the presence of deliberate (e.g., cyberattacks) or unintentional abnormal events. The adaptive isolation logic is event-triggered to avoid false positives, improve detection accuracy, and reduce computational overheads. A measurement-based stable kernel representation (SKR) triggering mechanism inspects distributed generation controllers for abnormal behavior. The SKR notifies a machine learning (ML) ensemble classifier that detects whether the system behavior is within acceptable operational conditions. The event-triggered adaptive isolation framework is evaluated using IEEE RTS-24 bus system. Simulation results demonstrate that the proposed framework detects anomalous behavior in real-time and identifies stable partitions minimizing operating costs faster than traditional islanding detection techniques.

Index Terms—Attacks, detection, distributed generation, event-triggered, islanding, isolation, resilience.

NOMENCLATURE

Constants:

χ_g	Power output growth rate for generator g .
λ	Weighting factor for the islanding objective function.
ω_g	Generator capacity weight for generator g .
$\omega_{l_{i,j}}$	Power flow weight of line $l_{i,j}$.
θ_d	Portion (%) of critical loads comprising load d .
B	Set of buses in system.
B^h, B^u	Buses in the healthy, unhealthy partitions.
D	Set of loads in system.
G	Set of generators in system.
L	Set of lines in system.
L^+, L^-	Set of inbound, outbound lines for a bus.
L^\bullet	Set of uncertain lines in system.
N	Set of nodes in system.
P_d^a	Aggregated power demand by load d .
P_g^{max}	Maximum power provided by generator g .
$P_{l_{i,j}}^{max}$	Maximum load flow for line $l_{i,j}$.
P_g^{min}	Minimum power provided by generator g .
$P_{l_{i,j}}^{min}$	Minimum load flow for line $l_{i,j}$.

Indices:

d	Index of load.
g	Index of generator.
i, j	Index of node.
$l_{i,j}$	Line connecting nodes i and j .

Variables:

β_d	Portion (%) of the served load demand of d .
ϕ_g	Binary decision variable for generator status.
h_b	Binary decision variable for bus b .

P_d^s	Power supplied to to load d .
$w_{l_{i,j}}$	Binary decision variable for line $l_{i,j}$.

I. INTRODUCTION

In recent years, the high penetration of renewable and distributed generation (DG) has altered the structure of traditional energy systems. The considerable advantages that active and/or autonomous, e.g., microgrids (MG), distribution systems offer – with respect to reliability, economic operation, energy loss minimization, and resilience to adverse events – justify the thrust towards a decentralized grid architecture. The interoperability of such architectures requires careful consideration for the orchestration of DG-integrated energy systems, especially during unexpected events, e.g., faults, cyberattacks, etc.

To overcome contingencies arising from unanticipated incidents, intentional controlled islanding (ICI) has been widely adopted in the literature, enforcing the sectionalization of the grid topology into healthy and supply-adequate islands [1], [2]. Numerous techniques have been proposed for the detection of islanding conditions [3]–[9]. Such techniques rely on remote or local measurements. Remote measurement-based schemes often require continuous and reliable information aggregation from system assets (e.g., generation facilities, distribution substations, etc.) to make informed islanding decisions. As a result, remote detection schemes become impractical, computationally intensive, or cost-prohibitive since they require the expansion of the communications infrastructure to account for changes in the energy network topology [10]. On the other hand, islanding techniques that rely on local measurements arise as more practical, cost-effective, and also faster in detecting islanding events [9], [11]. Abnormal conditions are determined by observing real-time system characteristics and classifying operational patterns into anomalous or expected behavior [11].

Islanding methods relying on local measurements are also classified into passive, active, and hybrid, based on the type of system data analyzed for anomaly identification. Passive methods examine system parameters such as the voltages and currents of DGs, frequency, total harmonic distortion, angles, etc., before making islanding decisions [12]. On the other hand, active islanding detection techniques monitor the system response to artificially injected perturbations introduced to the system [13], [14]. To improve islanding detection accuracy and avoid decision uncertainty, hybrid methods have also been proposed where passive and active techniques are used in coordination [15]. However, all the aforementioned islanding methodologies suffer from certain disadvantages. For example, passive methods have been proven to be less accurate when active power mismatch is negligible [15]. Active islanding detection requires specific instrumentation increasing the cost and could affect grid properties introducing voltage perturbations or degrading power quality [12]. Similarly,

TABLE I
ISLANDING DECISION SPEED AND ACCURACY OF MACHINE LEARNING
(ML) CLASSIFICATION ALGORITHMS

Algorithm	Speed	Accuracy	Reference
Phase space transform + PNN	0.230 sec	100%	[3]
ESPRIT	0.150 sec	95.6%	[4]
Classification + Regression tree	0.125 sec	94.45%	[5]
DWT + PNN	0.100 sec	90%	[6]
Decision Trees + DWT	0.024 sec	98%	[7], [8]
Extreme learning machines	0.021 sec*	99.3%*	[9]
SKR trigger + SVM ensemble	0.022 sec†	100%	This work

*Average based on reported results. †Worst-case scenario results.

although hybrid methods enhance detection confidence, they typically operate as a two-step process using passive methods as the first detection scheme, and only if passive methods are inconclusive do they revert to active methodologies [15]. Thus, improved accuracy comes at the cost of slower detection response times and more sophisticated detection equipment [3].

This performance trade-off has motivated multiple research works that harness the advantages of passive islanding methods, e.g., fast detection time, minimum hardware additions, no impact on grid operations, etc., and the availability of local measurements in DG and inverter-based resources (due to the decentralization of electric grids). Machine learning (ML) methods have also been employed to ameliorate some of the potential pitfalls of fusing passive islanding methods (e.g., greater non-detection zones) with local measurements for prompt and accurate islanding detection. For example, the authors in [9] train a group of randomized neural networks, called extreme learning machines (ELM), to perform event classification and decide whether islanding should be performed. In [6], discrete wavelet transformations (DWT) are used to extract features that are being provided to a probabilistic neural network (PNN) responsible for making islanding decisions. Leveraging a phase-space transformation technique combined with a PNN, the authors in [3] achieve fast and accurate islanding detection. The authors in [5] use data mining approaches to extract critical information from system parameter data sets, which are then forwarded to a classification and regression tree (CART) algorithm that classifies incidents and identifies conditions for islanding or non-islanding actions. Pattern recognition using decision tree (DT) classifiers trained on features extracted leveraging DWT have also been used due to their simple architecture allowing for fast detection [7], [8]. In [4], a naive Bayes classifier was trained to detect islanding conditions on measurement data preconditioned by estimating signal parameters via the rotational invariance technique (ESPRIT).

The aforementioned detection techniques, summarized in Table I, leverage ML and passive islanding classifiers to make fast and accurate decisions. They conform with industrial standards such as UL 1741 and IEEE 1547-2018 defining rules and requirements for anti-islanding protection schemes [16]. For instance, all techniques can detect islanding conditions within the 2 sec interval specified by IEEE 1547-2018. Apart from the detection speed and accuracy, the computational requirements for each method and its adaptability to grid topol-

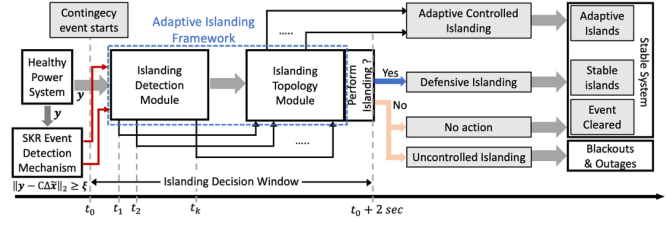


Fig. 1. Overview of the event-triggered islanding framework.

ogy changes should also be considered. Detecting islanding conditions in real-time on the DG inverter controllers can be challenging due to the limited computational resources of such devices. Additionally, the dynamic behavior, expansion, and reconfiguration of energy networks should be factored in when developing detection algorithms. As a result, event-triggered topology agnostic algorithms that use local measurements and can adapt to these changes (without requiring ML classifiers to be retrained or constantly monitor grid behavior increasing computations) are essential.

This work proposes an event-triggered adaptive islanding framework that comprehensively addresses the disadvantages of previous works. In Fig. 1, we present an overview of the proposed detection and isolation framework. Specifically, the first step includes the event-triggered detection of islanding conditions leveraging local measurements (i.e., passive islanding), support vector machine (SVM), and ensemble classifiers. As a result, computational-intensive ML tasks are only performed after an event has been triggered, reducing performance overheads.

The second step of the framework identifies stable island partitions of the grid topology in an adaptive manner while minimizing costs (e.g., load shedding, uneconomic generator operation, etc.). Namely, the adaptive islanding framework is composed of two distinct computational blocks, i.e., *i*) the islanding detection module and *ii*) the optimal islanding topology identification module, which work in parallel (Fig. 1). The aforementioned computational blocks work independently, and the detection module notifies the optimal islanding algorithm as soon as an anomaly is detected. Thus, the objective of the second step of the framework is first to detect anomalous incidents, and then determine supply-adequate islands while maximizing the size of the unhealthy partition (i.e., the one where the adverse incident is identified). After the islanding, if the contingency persists, the decided islands will be adaptively segregated into smaller autonomous partitions containing the impact of the adverse event. The contributions are as follows:

- 1) An event-triggered anomaly indication mechanism that identifies deliberate (e.g., cyberattacks) or accidental (e.g., faults) events. The event detection employs a stable kernel representation (SKR) of the system using local measurements aggregated at the DG inverters' side.
- 2) An ensemble classifier (after an event is triggered) to identify whether islanding should be performed. The voting classifier combines results from multiple consecutive rounds to ensure that correct decisions are made.
- 3) An automated scheme to provide adaptive islanding

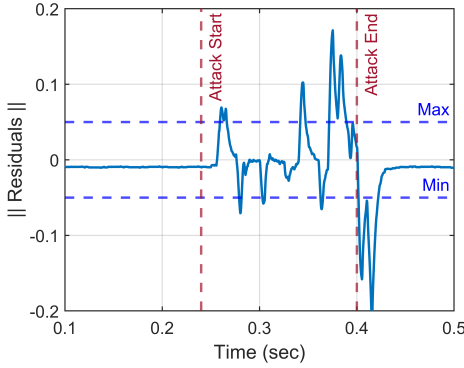


Fig. 2. Response of the SKR event detection schemes during a control input attack targeting DG inverter controller.

decisions minimizing operating costs and maximizing the size of the stable grid partitions. A case study on the IEEE RTS-24 bus system has also been included to demonstrate the efficacy of the proposed scheme in maintaining economic and stable grid operations.

The rest of the paper is organized as follows. Section II presents the event-triggered anomaly indication mechanism that prompts the islanding detection and isolation framework described in Section III. Simulation results and comparisons with other works are furnished in Section V. Section VI concludes the paper and provides directions for future work.

II. DISTRIBUTED EVENT-TRIGGERED ANOMALY INDICATION MECHANISM

In this section, we provide the preliminary definitions for the SKR extraction from the system model. We also elucidate the operation of the SKR event detection mechanism that supports the event-triggered functionality furnished by our adaptive isolation logic.

A. Distributed Generation System Model Dynamics

According to the mathematical modeling in [17], the small signal model of an inverter-based DG subsystem can be represented as:

$$\mathbf{E}\Delta\dot{\mathbf{x}} = \mathbf{A}\Delta\mathbf{x} + \mathbf{F}\mathbf{r}_0 \quad (1)$$

where \mathbf{A} , \mathbf{E} , and \mathbf{F} are the system and parameter (singular) matrices, $\mathbf{x} = [\delta, \omega, \mathbf{i}_d, \mathbf{i}_q, \mathbf{i}_{dref}, \mathbf{i}_{qref}, \mathbf{v}_d, \mathbf{v}_q, \mathbf{P}, \mathbf{Q}, \mathbf{V}_d, \mathbf{V}_q, \mathbf{i}_x, \mathbf{i}_y, \mathbf{V}_x, \mathbf{V}_y]^T$, and $\mathbf{r}_0 = [\omega_0]^T$, respectively. \mathbf{E} and \mathbf{A} are sparse matrices of the following forms and are defined in Appendix A of [17].

$$\mathbf{E} = \begin{bmatrix} \mathbf{E}_1 & \mathbf{E}_2 \\ 0 & 0 \end{bmatrix} \quad \text{and} \quad \mathbf{A} = \begin{bmatrix} \mathbf{A}_1 & \mathbf{A}_2 \\ \mathbf{A}_3 & \mathbf{A}_4 \end{bmatrix} \quad (2)$$

According to [11] the state variable vector can be described as $\tilde{\mathbf{x}} = [\Delta\delta, \Delta\omega, \Delta\mathbf{i}_d, \Delta\mathbf{i}_q, \Delta\mathbf{i}_{dref}, \Delta\mathbf{i}_{qref}, \Delta\mathbf{u}_d, \Delta\mathbf{u}_q]^T$, which leads to a state space system equivalent of the following form:

$$\Delta\dot{\tilde{\mathbf{x}}} = \tilde{\mathbf{A}}\Delta\tilde{\mathbf{x}} \quad (3)$$

where $\tilde{\mathbf{x}} = [\tilde{x}_1, \dots, \tilde{x}_m]^T$ and

$$\tilde{\mathbf{A}} = (\mathbf{E}_1 - \mathbf{E}_2\mathbf{A}_4^{-1}\mathbf{A}_3)^{-1} (\mathbf{A}_1 - \mathbf{A}_2\mathbf{A}_4^{-1}\mathbf{A}_3) \quad (4)$$

The feedback controller of the system defined in (3) can be defined as:

$$\begin{cases} \mathbf{u} = \mathbf{K}\mathbf{y} \\ \mathbf{y} = \mathbf{C}\Delta\tilde{\mathbf{x}} \end{cases} \quad (5)$$

with $\mathbf{u} = [u_1, \dots, u_n]^T$ the control inputs, $\mathbf{y} = [y_1, \dots, y_n]^T$ the output measurement vectors, and $\mathbf{C} \in \mathbb{R}^{n \times m}$ being the output matrix. Ignoring system and process measurement noise, and combining Eqs. (1) - (5) the system model can be described as:

$$\begin{cases} \Delta\dot{\tilde{\mathbf{x}}} = \tilde{\mathbf{A}}\Delta\tilde{\mathbf{x}} + \mathbf{B}\mathbf{u} \\ \mathbf{y} = \mathbf{C}\Delta\tilde{\mathbf{x}} \end{cases} \quad (6)$$

The calculation of state space residuals (from Eq. (6)) can then be used for the detection of attacks, and data integrity violations targeting power systems [11], [18], [19].

B. Event-triggered Stable Kernel Representation Alarms

State residuals, \mathbf{r} , are defined as the deviation of real measurements \mathbf{y} and their corresponding estimated values $\mathbf{C}\Delta\tilde{\mathbf{x}}$ for the same system. Then leveraging a χ^2 -distribution with predefined degrees of freedom (e.g., system states) and confidence intervals (e.g., values within the 95% or 99% confidence interval) as indicated by the system model, we can define a static threshold ξ . If the residual deviation is greater than ξ , i.e., $\mathbf{r} = \|\mathbf{y} - \mathbf{C}\Delta\tilde{\mathbf{x}}\|_2 > \xi$, then the measurements are considered corrupted. Our methodology leverages the state residual deviations as an *anomaly indicator*. Instead of using static predefined thresholds ξ_i for each subsystem, we leverage system measurements to develop constantly updating dynamic thresholds that serve as inputs to the islanding detection module. Once a violation of the state residuals is detected, then control is handed over to the islanding detection module (Section III), which is responsible for identifying if a compromise or any other adverse event has occurred. This two-step approach reduces potential false positive alarms and conserves computation bandwidth since the distributed agents do not constantly monitor for anomalous events.

We illustrate the effectiveness of SKR in generating reliable alarm signals during anomalous conditions and its improvement over traditional passive detection methods in Fig. 2 and 3. The event detection is performed in the Canadian urban distribution feeder system benchmark, which comprises four DGs that, in our case, are inverter-based [17]. We employ a control input attack affecting the operation of a DG inverter controller as an illustrative example. The control input attack starts at 0.25 sec and finishes at 0.4 sec. In Fig. 2, the SKR triggering mechanism generates multiple abnormal event signals throughout the duration of the control input attack, proving its efficacy. On the other hand, as demonstrated in Fig. 3, even though some passive islanding techniques, e.g., rate-of-change-of-frequency (ROCOF), rate-of-change-of-voltage (ROCOV), rate-of-change-of-active/reactive power (ROCOAP/ROCORP) could also detect anomalous behavior, their detection speed and robustness (values exceeding thresholds) are significantly worse than the SKR that produced multiple alarms within this time frame. Furthermore, metrics like ROCOF could still keep providing false alarms even after

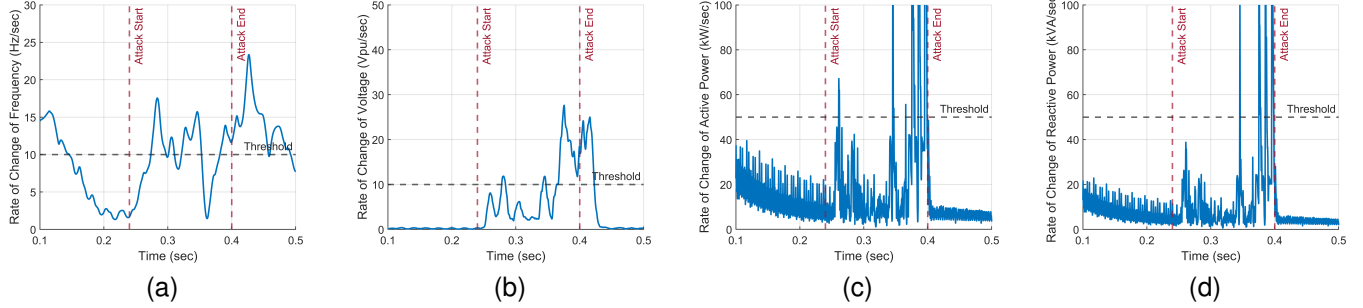


Fig. 3. Response of passive islanding detection schemes during a control input attack targeting DG 2, (a) rate of change of frequency (ROCOF), (b) rate of change of voltage (ROCOV), (c) rate of change of active power (ROCOAP), and (d) rate of change of reactive power (ROCOP).

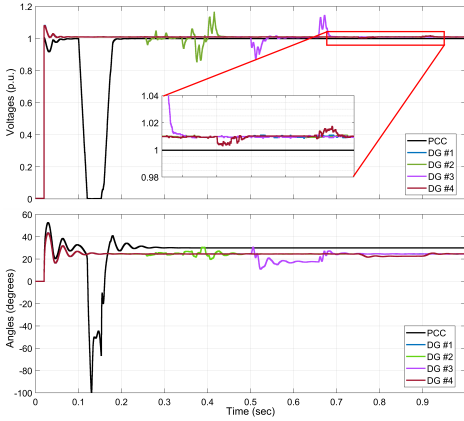


Fig. 4. Voltage and angles of the system during different adverse scenarios.

the attack has stopped, i.e., $t \geq 0.4$ sec, potentially triggering unintentional islanding.

We evaluate the efficiency of SKR alarm generation mechanism under diverse attack scenarios, derived from [9], including *i*) a three-phase fault at the point-of-common-coupling (PCC) between the DG and the main grid, *ii*) a control input attack, *iii*) a line-to-line fault, and *iv*) a 50% load altering attack. Notably, the three-phase fault takes place from 0.1 to 0.15 sec, the control input attack from 0.25 to 0.4 sec, the line-to-line fault from 0.5 to 0.65 sec and the load increase and decrease at 0.75 and 0.95 sec, respectively. The impact of the aforementioned abnormal conditions on the DG voltages and angles are presented in Fig. 4. Furthermore, the SKR event detection response is demonstrated in Fig. 5. All anomalous conditions, apart from the load deviation that does not compromise the system operation (also verified by Fig. 4), would trigger SKR alarms since they exceed operational thresholds.

III. ISLANDING DETECTION

In this section, we describe the data-driven procedure used for the detection of anomalous grid behavior and then present the methodology to enforce controlled islanding in an effort to minimize the net balance of power supply-demand. We provide some preliminary definitions of the system and the ML classifiers used for the detection stage of our framework and then delineate the adaptive decision-making process working in collaboration with our grid isolation logic.

A. Preliminaries

1) *Predictor and Outcome Variables*: In ML and statistics, different terminology can be used to describe similar concepts. For instance, the objective of a ML classification algorithm is to decide the class to which the observation belongs, i.e., to predict its label. To make such decisions, ML classifiers are “fitted” on samples of data; the data used to train them are commonly referred to as independent variables, predictors, or features. Similarly, the output of the ML classifier is called the dependent variable, the outcome variable, or the target. In summary, ML algorithms manipulate independent variables or predictors to explain how changes in independent variables affect dependent or outcome variables. For the rest of the paper, the aforementioned terms will be used interchangeably.

2) *Support Vector Machine Classifiers*: Support vector machines (SVMs) are supervised ML algorithms that have been used in different scientific disciplines for classification and regression tasks. To achieve its objective, e.g., classification, an SVM will attempt to identify a hyperplane or multiple hyperplanes that would optimally divide the dependent variables into different classes. Since SVMs are working with high-dimensional subspaces, multiple viable hyperplanes that properly classify a data set might exist. In such cases, SVMs will pick the hyperplane that achieves the highest margin, i.e., the biggest separation among classes.

SVMs can be used for both linear and non-linear classification, and depending on their objective, different kernel functions are employed. These kernel functions are responsible for evaluating the separating hyperplane margin. Although many potential kernel function candidates exist, e.g., linear, quadratic, polynomial, radial basis, etc., in our case, we have opted for a cubic and a Fine Gaussian (FGSVM) SVM kernel. Cubic SVMs have been proven to be effective classification algorithms that balance detection accuracy and speed [20], while FGSVM can achieve superior accuracy even when dealing with multi-domain feature spaces [21] as in our case.

3) *Ensemble Learning Classifiers*: Ensemble learning methodologies are used in ML and statistics to achieve better prediction results by combining multiple predictions from different models, also known as learners. Learners can be classified into weak or strong depending on their prediction performance on a given task. Combining the independent outcomes of multiple weak learning algorithms, strong learner

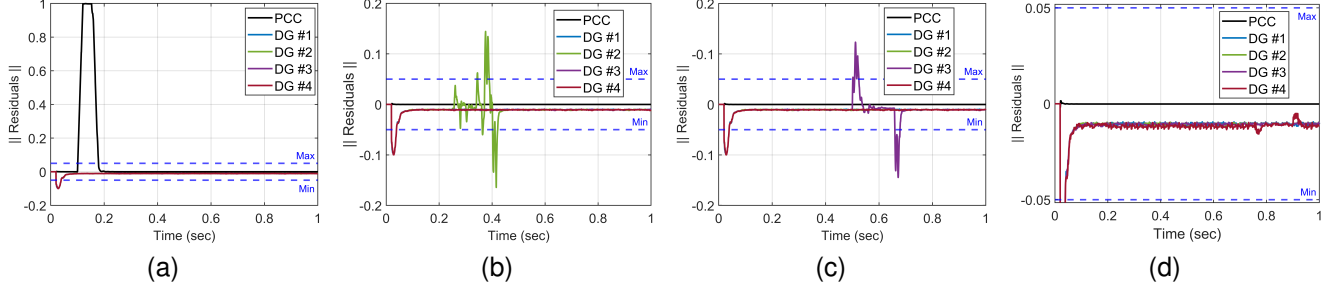


Fig. 5. Operation of SKR triggering mechanism for different abnormal scenarios, (a) three-phase fault at PCC, (b) control input attack at DG 2, (c) line-to-line fault at DG 3, and (d) 50% load deviation attack at DG 4.

Algorithm 1: Bagging Methodology.

Input: Training Set: $\mathcal{D} = \{\{\mathbf{x}_1, y_1\}, \{\mathbf{x}_2, y_2\}, \dots, \{\mathbf{x}_k, y_k\}\}$
Define \mathcal{N} = Number of training rounds
Define \mathcal{L} = Bagging Learner Model (e.g. Decision Tree)
Process:
for $t = 1, 2, \dots, \mathcal{N}$ **do**
 $h_t = \mathcal{L}(\mathcal{D}, \mathcal{D}_{sub})$
end
Calculate Class of Target
Output: $\mathcal{H}(\mathbf{x}) = \arg \max_{y \in \mathcal{Y}} \sum_{t=1}^{\mathcal{N}} \mathbb{I}(h_t(\mathbf{x}) = y)$

models can be formulated. Different methodologies are used for the combination of weak learner prediction results, the most popular being boosting, stacked generalization (stacking), and bootstrap aggregation (bagging) [22].

In boosting topologies, learners are trained sequentially, and the main focus of boosting algorithms is to minimize the prediction error that the previous stage learners exhibited. In contrast, stacking uses different model architectures of learners, i.e., level one learners, that are fitted on the data to infer the diverse characteristics of the training set, while a second-level learner model is used to combine the outputs of the level one learners. In bagging, multiple weak learners (typically using the same ML model, e.g., decision tree) are trained on different sections of the training data. Then, the outputs of these weak learners are combined to make prediction decisions (Algorithm 1).

After weak learners have reached an outcome, their predictions have to be combined to reach a decision, e.g., which class the dependent variable belongs to. Decisions can be made using simple statistical methods, such as averaging (for regression) or voting (for classification). In the voting case, different weights can be assigned to each learner based on its respective prediction accuracy. Regardless of the learner weights, two distinct voting schemes can be identified to assist in the decision-making process. In hard voting, voting is performed based on the predicted class of the dependent variable, while in soft voting, it is performed based on the probabilities of the predicted output class. For this work, we use a bagging, specifically bagged trees, hard voting ensemble classifier due to its faster, independent (contrary to boosting), and parallel training procedure, as well as its prediction speed [23].

B. Adaptive Islanding Detection Scheme

This section outlines the methodology of the islanding scheme.

1) *Feature Vector Models:* The islanding detection mechanism analyzes time series data collected from multiple sensors within the system, in our case the measurements are collected from the DG inverter controllers. For example, in the Canadian urban distribution feeder system, 54 features are used to predict anomalous behavior. These features include the DG local measurements (collected from their inverters), such as three-phase voltage, currents, and harmonic noises. Additionally, the per-unit voltages, frequencies, and angles reported at the system buses, the point-of-common-coupling (PCC), and the distribution lines are also incorporated in the feature vectors. In Eq. (7), we formulate a generalized version of the input feature vector \mathbf{x} , where \mathcal{K} and \mathcal{N} refer to the number of measurement points and the number of DGs (providing local measurements), respectively. The voting ML classifier is then trained to fit the aggregated measurements compiled in the feature vectors.

$$\mathbf{x} = [v_{pu}^1, v_{pu}^2, \dots, v_{pu}^{\mathcal{K}}, \delta^1, \delta^2, \dots, \delta^{\mathcal{K}}, f^1, f^2, \dots, f^{\mathcal{K}}, v_{abc}^{DG1}, i_{abc}^{DG1}, thd_{abc}^{DG1}, v_{abc}^{DG2}, i_{abc}^{DG2}, thd_{abc}^{DG2}, \dots, v_{abc}^{DGN}, i_{abc}^{DGN}, thd_{abc}^{DGN}] \quad (7)$$

These features will be mapped by ML classifiers (i.e., cubic SVM, FGSVM, DTs, etc.) in a high-dimensional space where changes in any of these predictors will be associated with nominal or abnormal system operation. As a result, the system behavior and the evolution of its dynamic state trajectories will be directly correlated with the measured data points (within the feature vectors). Our methodology uses raw data allowing the dynamic update of our learning models without requiring data preconditioning steps (decompressing encoded data [9], [24]) – adding complexity and computations – while overcoming potential reconstruction issues for post-event analyses, since the feature vectors might not be reversible (e.g., lossy encoding).

2) *Training Process:* The feature vectors are forwarded to the learning algorithms described in Sections III-A2 and III-A3 to train the islanding detection classifiers. The training of the classifiers is performed independently (and in parallel). In Table II, we compile information on the structure and the specific characteristics of the learning algorithms. Each corresponding algorithm enhances the fitting capabilities of the combined classifier since cubic and Gaussian kernel functions,

TABLE II
MACHINE LEARNING (ML) CLASSIFICATION ALGORITHM
SPECIFICATIONS

Learner Model	Parameter	Value
Bagged Trees	Ensemble Method	Bootstrapping Aggregation
	Learner Type	Decision Tree
	# of Learners	30
	Max # of Splits	200k
	Miss-classification cost	unweighted
Cubic SVM	Kernel Function	Cubic
	Kernel Scale	1.0
	Miss-classification cost	unweighted
Fine Gaussian SVM	Kernel Function	Fine Gaussian
	Kernel Scale	1.8
	Miss-classification cost	unweighted

as well as bagged decision trees, learn to predict how changes in features are reflected on the dynamic system states. It should be highlighted that learner training is an offline process that can be time-consuming depending on the dimension of the feature vectors and the size of the training dataset. Although training is not carried out in real-time, the detection of anomalous events is going to be performed respecting the real-time power system constraints.

3) *Classification Process*: The islanding detection is a two-stage classification process. During the first stage of the classification, the three distinct learner algorithms decide independently whether the input time series data, i.e., features, correspond to nominal or abnormal operation. After the inference stage, the results of each individual classifier are forwarded to the voting algorithm, where by majority vote, the final decision for the label of the input data is made. The credibility of the final decision is validated on a rolling window basis, which comprises the second stage of the classification process.

The second stage of the classification process aggregates the results from each individual classifier and, by averaging the three latest decisions, identifies the correct class. Given that our classifiers can make real-time decisions on the input data in less than 0.022 *secs*, we aggregate the inference results over three consecutive rounds forming the cumulative confidence score (Fig. 6). If the decisions of independent classifiers are found to be consistent in the class of input measurements, i.e., decision credibility (Fig. 6) is higher than 90%, then this decision is considered credible and is forwarded to the optimal islanding module, which will take the corresponding actions based on the classification results [9].

If consensus between individual classifiers is not reached within the three predefined rounds, i.e., decision credibility is less than 90%, the rolling decision window is extended to five rounds. After the fifth round, the average decision is forwarded to the islanding module (regardless of the decision accuracy). Based on our simulation results, the proposed islanding detection mechanism can achieve an accurate decision, with a longer decision interval. However, faster and accurate detection can allow the islanding module to calculate the optimal adaptive islanding topology, minimizing power-demand imbalances and, at the same time, limiting the potential impacts of adverse events (restricting the impact

Algorithm 2: Classification Methodology.

Input: Feature Vector: \mathbf{x}_t , Trained Classifiers C_i

Define \mathcal{NR} = Number of decision rounds

Define \mathcal{NC} = Number of decision classifiers

Process:

$score = 0; credibility = 0;$

for $t = 1, 2, \dots, \mathcal{NR}$ **do**

$score = score + C_1(\mathbf{x}_t) + C_2(\mathbf{x}_t) + \dots + C_{\mathcal{NC}}(\mathbf{x}_t)$

if $t == 3$ **then**

$credibility = score \div (3 \times \mathcal{NC})$

if $credibility \in [0, 0.1]$ **OR** $credibility \in [0.9, 1]$ **then**

$\mathcal{Y}_{[k, k+t]} = round(credibility)$

break;

end

end

$\mathcal{Y}_{[k, k+t]} = round(score \div (\mathcal{NR} \times \mathcal{NC}))$

Decide Class of Event

Output: $\mathcal{Y}_{[k, k+t]}$

propagation to just a subpart of the whole system). Algorithm 2 describes the classification and the inference of event class labels (i.e., normal or abnormal system states).

IV. MIXED INTEGER LINEAR PROGRAMMING ISLANDING METHODOLOGY

In this section, we present the mixed integer linear programming (MILP) islanding process formulation. In more detail, the proposed methodology aims to identify stable regions, i.e., islands, while maximizing the served load demand. The network topology of the power system can be modeled as an undirected graph (N, L) consisting of $|N|$ nodes and $|L|$ lines representing the branches that connect the system buses included in B . The direction of the edges of the graph is arbitrarily chosen and is not of interest to our methodology, similarly to other research works [25], [26]. The set of generators and loads in the system are represented by G and D , respectively. In the following, we will present the binary variables and the constraints that the optimizer aims to satisfy while minimizing load losses.

A. Islanding Constraints

1) *Generator Constraints*: The output of the generators within the system is limited by their absolute minimum and maximum ratings as well as their steady-state and transient response characteristics. During an islanding event, a generator could either be completely disconnected (switched off) or operated within a feasible margin around its previous steady-state point due to its physical limitations (e.g., recovery response):

$$P_g[1 - \chi_g(P_g - P_g^{min})] \leq \phi_g P_g \leq P_g[1 + \chi_g(P_g^{max} - P_g)] \quad (8)$$

where ϕ_g is a variable that models if generator g is switched on ($\phi_g = 1$) or off ($\phi_g = 0$). If generator g is still running, its power output P_g will be within its operating limits, that is, between P_g^{min} and P_g^{max} .

2) *Load Constraints*: During an islanding event the power system is sectionalized into healthy and unhealthy sections. As a result, some loads might not be able to be served due

to generator limitations, e.g., generators might have reached their maximum capacity, or line constraints (maximum power flow reached). In such occasions, load shedding is performed to maintain the stability of the sectionalized areas. We use a load aggregation model to represent this relationship:

$$P_d^s = \beta_d P_d^a \quad s.t. \quad \theta_d \leq \beta_d \leq 1 \quad (9)$$

where θ_d represents the portion of the aggregate load d that is critical, i.e., has priority in being served during an islanding, and β_d is the actual portion of loads being supplied. If $\beta_d = 1$, the entire demand is satisfied by the resources of the corresponding section of the power system to which d belongs.

3) *Line models and constraints*: For our line modeling, we have opted for a AC power flow model. As a result, for our system to attain stability pre or post islanding:

$$\forall b \in B : \sum_{g \in G} P_g + \sum_{l_{i,j} \in L^+} P_{l_{i,j}} - \sum_{l_{i,j} \in L^-} P_{l_{i,j}} = \sum_{d \in D} P_d^s \quad (10)$$

Apart from Eq. (10), the power flow network should not be overloaded (especially post islanding). Thus, the real power flow line limits, i.e., *MW* ratings, should not be exceeded:

$$P_{l_{i,j}}^{min} \leq w_{l_{i,j}} P_{l_{i,j}} \leq P_{l_{i,j}}^{max} \quad (11)$$

B. Islanding Formulation

To effectively perform islanding, once a maloperating part of the system is identified, the grid topology needs to be segregated into healthy and unhealthy network partitions. The healthy system portion will encompass all the nodes that are operating nominally, while the unhealthy partition is defined as the maximum allowable network partition proposed by our islanding strategy. To distinguish between buses that exist in healthy and unhealthy network partitions, we utilize the binary decision variable h_b . Such that:

$$\forall b \in B : \begin{cases} h_b = 1 & | b \in B^h \subseteq B \text{ (healthy part)} \\ h_b = 0 & | b \in B^u \subseteq B \text{ (unhealthy part)} \end{cases} \quad (12)$$

We use another binary decision variable, i.e., $w_{l_{i,j}}$, for the lines that will remain connected after partitioning the network topology into healthy (B^h) and unhealthy (B^u) subsets. It should be noted that disconnected lines with both ends in B^h could also exist (e.g., if they reach their power flow limits). We denote with $L^\bullet \subseteq L$ the set of lines that should be disconnected as a result of physical (e.g., ratings), other limitations (e.g., connecting healthy and unhealthy islands), or could potentially cause power instabilities. The following describes the relation between line connectivity and binary variable $w_{l_{i,j}}$.

$$\forall l_{i,j} \in L, i, j \in N : \begin{cases} w_{l_{i,j}} = 1 & | l_{i,j} \text{ (line connected)} \\ w_{l_{i,j}} = 0 & | l_{i,j} \text{ (line disconnected)} \end{cases} \quad (13)$$

Additional constraints exist for the lines belonging to L^\bullet . Such lines should be disconnected if they are connecting B^h and B^u . That is,

$w_{l_{i,j}} = 0 : \forall l_{i,j} \in L | h_{b_i} = 1, h_{b_j} = 0$ or $h_{b_i} = 0, h_{b_j} = 1$. Furthermore, if both ends of the line exist in B^h , the line should also be disconnected to maintain the stability of B^h .

On the other hand, if both ends of the line exist in B^u , i.e., $h_{b_i} = 0$ and $h_{b_j} = 0$, the line can remain connected since the stability of B^u cannot be guaranteed during islanding. The aforementioned constraints can be modeled by the following inequalities.

$$\forall l_{i,j} \in L^\bullet : w_{l_{i,j}} \leq 1 - h_{b_i} \text{ and } w_{l_{i,j}} \leq 1 - h_{b_j} \quad (14)$$

For the remaining lines, i.e., $l_{i,j} \in L \setminus L^\bullet$, we still have to ensure that if they connect B^h and B^u they need to be disconnected. However, in this case, if a line $l_{i,j}$ belongs exclusively to B^h or B^u , it can either remain connected or disconnected without affecting the stability of the islands. These constraints are formalized by the following inequalities.

$$\forall l_{i,j} \notin L^\bullet : w_{l_{i,j}} \leq 1 - h_{b_i} + h_{b_j} \text{ and } w_{l_{i,j}} \leq 1 + h_{b_i} - h_{b_j} \quad (15)$$

C. Islanding Objective Function

The objective of defensive islanding is to divide the power grid into stable islands while serving as many critical loads as possible (minimizing load imbalances). Typically, these islands are composed of generators that furnish similar angles before the islanding process is initiated, i.e., generator coherency. Apart from the optimal generator groupings efficiently meeting load demand, minimizing the number of line disconnections guarantees that the grid architecture (post-islanding) will be able to withstand potential future disturbances and cascading accidental or deliberate contingencies. The formulations provided in Eq. (16a), (16b), and (16c) model the aforementioned three objectives.

$$\min \sum_{l_{i,j} \notin L^h} w_{l_{i,j}} (1 - w_{l_{i,j}}) \quad (16a)$$

$$\min \sum_{g \in G} \omega_g (1 - \phi_g) \quad (16b)$$

$$\max \sum_{d \in D} \beta_d P_d^a [h_d + \psi_d (1 - h_d)] \quad (16c)$$

In Eq. (16a) we constrain the optimizer to minimize the number of lines that will be disconnected (through the term $1 - w_{l_{i,j}}$) and the number of generators that are going to be disconnected is similarly minimized in Eq. (16b) through the $1 - \phi_g$ term. The weights $w_{l_{i,j}}$ and ω_g are normalized based on the maximum allowable line power flow and generator nameplate capacity to keep connected lines and generators with ‘‘heavier’’ weights. In Eq. (16c) maximizing the loads being served and minimizing the size of the unhealthy network topology are jointly optimized via the $[h_d + \psi_d (1 - h_d)]$ term. ψ_d is a stochastic variable modeling the probability of a load d belonging in the B^u to be served. Since $0 \leq \psi_d \leq 1$, $\beta_d P_d^a \psi_d \leq \beta_d P_d^a$, thus, priority is given to the loads attached to buses in B^h . Combining the previously described equations gives us the comprehensive form of the islanding objective function presented in Eq. (17).

$$J = \max(\lambda_1(16c) - \lambda_2(16a) - \lambda_3(16b)) \quad (17)$$

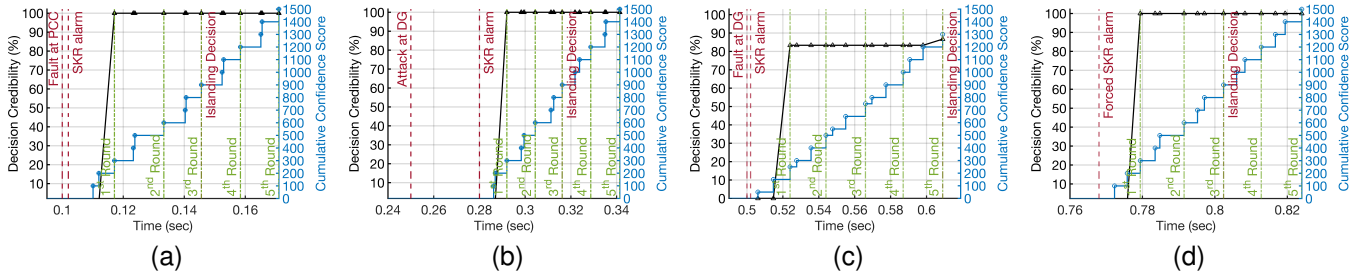


Fig. 6. Operation of the detection mechanism for different scenarios, (a) three-phase fault at PCC, (b) control input attack at DG, (c) line-to-line fault at DG, and (d) 50% load deviation attack at DG.

Here $\lambda_1, \dots, \lambda_3$ are positive weights, uniformly selected in our case, used to prioritize sub-objectives (Eq. (16a), (16b), and (16c)) of the optimizer while improving its convergence (limiting the size of the branch and bound space).

V. SIMULATION RESULTS

In this section, we compile results for the adaptive controlled islanding framework and demonstrate the impact that different islanding strategies have on the IEEE 24-bus network. We present results for the event-triggered detection and compare the proposed proactive islanding method – that aims to maintain large supply-adequate islands – with common islanding schemes that aim to aggressively isolate compromised grid sections. The efficiency of these adaptive islanding is evaluated using AC power flow solutions.

A. System Model

In this study, the IEEE 24-bus reliability test system (RTS) is used to evaluate the isolation logic. RTS is composed of 24 buses, 38 branches, 17 aggregated loads, and 32 generators (comprising the 10 generators shown in Fig. 7a). The total generation capacity of the RTS is 3075 MW, while the net demand from its 17 loads is equal to 2850 MW. More information, including the generator start-up, shutdown, operating costs, etc., and the specifics of the RTS 24-bus system, can be found in [27]. Similar scenarios to the ones employed in [9], i.e., best algorithm with respect to detection speed and accuracy, are used for the evaluation of our islanding methodology. Specifically, the scenarios that we aim to detect for potential islanding include: *i*) fault at PCC at bus 1, *ii*) attack at bus 1 (simulated a control input attack), *iii*) fault and trip of bus 4, *iv*) load altering attack (increase by 50%) at bus 4. Buses 1 and 4 have been arbitrarily chosen, and similar detection results would be triggered for any other generation or load bus of the system under test. Furthermore, the scalability of our proposed methodology can be guaranteed, given that the SKR event triggering and the islanding detection are performed distributively (by the corresponding system bus/agent, e.g., DG controller). As a result, single-points-of-failure, e.g., central nodes aggregating system measurements, are avoided, and system nodes requiring advanced computational resources (to act upon the aggregated measurements) are not essential. Last, system operator involvement is only necessary for the sectionalization commands (not the detection).

B. Islanding Detection

In this section, we evaluate the effectiveness of the SKR event-triggered and ensemble-based detection scheme for the four scenarios introduced in Section II-B and Fig. 5 based on [9]. In more detail, Fig. 6 demonstrates the operation of the event-triggered detection combining the SKR alarms and voting ensemble classifier (Algorithm 2). The cumulative confidence score (vertical right axis) indicates the confidence of the islanding classification results over consecutive decision rounds. Based on the credibility percentage of the classifier outcomes drawn in each corresponding round (vertical left axis), islanding (or not) is performed if decision credibility $\in [0.9, 1.0]$, as described in Algorithm 2. To balance decision accuracy and detection speed, islanding decisions are either made during the third or fifth round. It should be noted that in both scenarios (third or fifth round), decisions are promptly made (faster than 2 *secs*), conforming with IEEE-1547. Faster than real-time detection is essential, and our methodology guarantees that (for each round) classification can be performed in less than one cycle of a 50/60 Hz system (on average), i.e., 0.02/0.017 *secs* respectively. Thus, allowing the final decision to be formed leveraging incoming measurements that are progressively received by the classifiers.

Specifically, in the scenarios illustrated in Figs. 6a, 6b, 6c, it can be seen that after the four adverse conditions are initiated (per Section II-B), the SKR alarms are issued. Contrary to the fault scenarios Figs. 6a and 6c, which are immediately detected, the stealthy control input attack requires more time for the alarm generation. On the other hand, in the load increase scenario, Fig. 6d, no SKR alarm would be generated since such an event would not compromise the system operation (Fig. 5d). Notably, the SKR alarm would not be triggered in this scenario since there is sufficient generation to cope with the 50% load deviation attack. To illustrate the robustness of our detection mechanism, even if an erroneous alarm signal has been generated, i.e., a false positive, we have manually issued a synthetic SKR alarm. The ensemble voting classifier is able to make a correct islanding decision even in the presence of this “forced” alarm that we issue at 0.77*sec*.

Regarding the islanding detection accuracy of the ensemble-based classifier, Accurate decisions are made in three decision rounds in all use cases, apart from the line-to-line fault, where two more rounds are necessary for the identification of this abnormal condition. Notably, in every scenario (even the forced

one in Fig. 5d), accurate decisions are made. Furthermore, the per-round detection time necessary to draw decisions of our proposed methodology is superior to previously reported studies, furnished in Table I. Namely, when comparing our work with the results reported by [3]–[8] or [9], which also leverages a voting classifier, we can guarantee higher detection accuracy and faster detection speeds, i.e., 0.008 *secs* average and 0.022 *secs* maximum value versus 0.021 *sec* (per round).

C. IEEE RTS-24 Adaptive Islanding Test Case

We validate the practicality of our approach using the IEEE RTS-24 system, where multiple islandings should be performed in succession. As presented in Fig. 1 the islanding detection and topology modules support the adaptive control islanding scheme that aims to identify the optimal stable topology sectionalization strategy (following Eqs. (8)–(17)). After the detection of a maloperating bus, the healthy and unhealthy partitions of the system, defined by the adaptive control islanding methodology, should be able to maintain the critical portion of the power demand.

In more detail, for our use case, we assume that bus 4 in Fig. 7a has been compromised. After the abnormal operation of bus 4 has been detected, the adaptive controlled islanding module will select an optimal topology to sectionalize the RTS-24 system into two stable partitions. We will refer to the partition, including the anomalous agent (bus 4), as the unhealthy partition ($\forall b \in B^u$). The healthy partition consists of all the remaining buses, i.e., $B^h : \forall b \notin B^u$. In Fig. 7b, we can see how the system is partitioned following the islanding methodology presented in Section IV. We opt for larger islands instead of aggressively identifying the minimum size cut of the topology graph that will include the anomalous node (bus 4) and have sufficient generation to meet the island’s power demand.

Traditional islanding methodologies would attempt to create a section including the compromised bus 4 as well as buses 1, 2, 7, 8, 9, 11, 12, 13, which would satisfy the generation-demand balance of the island. Specifically, the P_{GEN}, Q_{GEN} are 1245MW and 1275MVA respectively, while the demand values are P_{DEM}, Q_{DEM} are 1088MW and 221MVA. However, this topology would create load imbalances in the rest of the system and increase operational costs. Other islanding topologies, including buses 1, 2, 4, 7, 8, 9 or 1, 2, 4, 5 would require load sheddings since the generation would not be sufficient to meet load demands but would also congest lines such as lines 1-2 and 7-8.

The proposed method identifies “larger” stable islands while avoiding uneconomical operation, line congestion, and load shedding. The details of the nominal system, i.e., before islanding, as well as the corresponding two islands created after the detection of the malicious agent (Fig. 7b), are presented in Table III. Leveraging the AC power flow solution and the generator cost information provided in [27], we can calculate that before the islanding the cost of operating the whole system was \$36418.68, while after the islanding, the aggregated cost is \$36436.05 (0.05% increase). Furthermore, both islands 1 and 2 have sufficient generation and reserves to meet the current demands and potential future load increases.

TABLE III
STEP-1 OF ADAPTIVE CONTROLLED ISLANDING

	Nominal	Island 1	Island 2
Buses	1-24	3, 14-19, 21, 21, 24	1, 2, 4-13, 20, 23
P_{GEN}^{max}	3075 MW	1470 MW	1605 MW
P_{DEM}^{max}	2850 MW	1305 MW	1545 MW
Q_{GEN}^{max}	3055 MVA	1470 MVA	1585 MVA
Q_{DEM}^{max}	580 MVA	265 MVA	315 MVA
Lines Disc.	-	1-3, 3-9, 11-14, 19-20	
Cost	\$ 36418.68	\$ 9976.68	\$ 26459.37

TABLE IV
STEP-2 OF ADAPTIVE CONTROLLED ISLANDING

	Island 1	Island 2a	Island 2b
Buses	3, 14-19, 21, 21, 24	2, 4, 7-9	1, 5, 6, 10-13, 20, 23
P_{GEN}^{max}	1470 MW	502 MW	1103 MW
P_{DEM}^{max}	1305 MW	642 MW	903 MW
Q_{GEN}^{max}	1470 MVA	492 MVA	1093 MVA
Q_{DEM}^{max}	265 MVA	131 MVA	184 MVA
Lines Disc.	1-3, 3-9, 11-14, 19-20	1-2, 2-6, 8-10, 9-11, 9-12	
Load Shed	0%	30.3%	0%
Cost	\$ 9976.68	\$ 8234.64	\$ 25934.57

In cases where contingencies persist, the evolutionary stage of the adaptive islanding methodology will attempt to partition the unhealthy part of the system into smaller islands while meeting operational constraints. Fig. 7c demonstrates how island 2 would be further partitioned if bus 4 cannot be recovered and continues to operate abnormally. Island 2 is segregated into island 2a (unhealthy) and island 2b (healthy). The specific generation details for the aforementioned islands are summarized in Table IV. It should be noted that in cases where the system constraints do not allow the design of two stable (supply-adequate) islands, the methodology prioritizes the formation of a bigger healthy partition (avoiding load shedding in this section) as defined by Eqs. (14),(15), and (16c).

As a result, island 2b is able to supply the load buses in the topology indicated using blue colors in Fig. 7c. However, island 2a, i.e., the persistent unhealthy system partition, should perform load shedding to continue its operations. In more detail, 30.3% of the loads located in island 2a, have to be shed due to the imbalance between P_{GEN} and P_{DEM} , which are 502MW and 642MW, respectively. Furthermore, regardless of the cost of load shedding, the generators in island 2a have to operate at their maximum capacity, increasing the overall cost of operating island 2 from \$26459.37 to \$34169.21 (29.1% increase).

VI. CONCLUSIONS AND FUTURE WORK

In this work, we explore the concept of islanding to answer the questions of *when*, *where*, and *how* to deal with unexpected grid contingencies. We utilize an SKR event triggering scheme that serves as the input to the islanding detection module, balancing detection speed, accuracy, and computational resources at the DG edge. Once an anomalous condition is detected, the adaptive islanding topology module generates supply-adequate sections minimizing operating costs. Our future work will

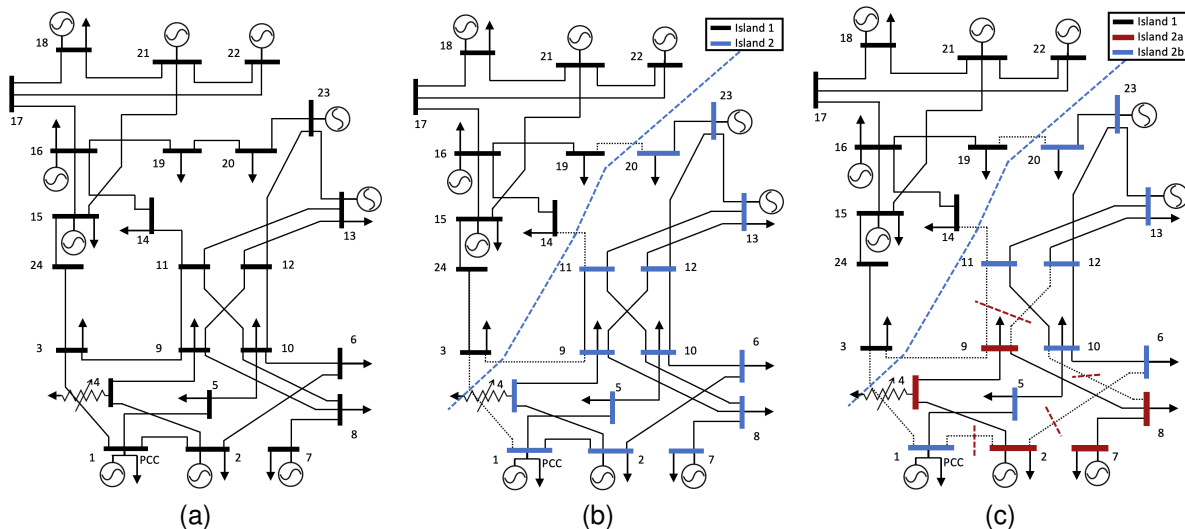


Fig. 7. Modified RTS24 bus system including the controllable load at bus 4 and the PCC connection at bus 1. (a) Nominal system, i.e., pre-islanding, (b) first step of adaptive islanding due to malicious operation at bus 4, and (c) second step of adaptive islanding due to the persistence of the adverse conditions at bus 4, leading to load shedding.

focus on how mobile battery energy sources can be optimally deployed to enhance the proposed scheme, overcome potential load shedding, and maintain reserves in case of cascading adverse events.

REFERENCES

- [1] J. Quirós-Tortós, R. Sánchez-García, J. Brodzki, J. Bialek, and V. Terzija, "Constrained spectral clustering-based methodology for intentional controlled islanding of large-scale power systems," *IET Generation, Transmission & Distribution*, vol. 9, no. 1, pp. 31–42, 2014.
- [2] P. Demetriou, M. Asprou, and E. Kyriakides, "A real-time controlled islanding and restoration scheme based on estimated states," *IEEE Transactions on Power Systems*, vol. 34, no. 1, pp. 606–615, 2018.
- [3] A. Khamis, H. Shareef, and A. Mohamed, "Islanding detection and load shedding scheme for radial distribution systems integrated with dispersed generations," *IET Generation, Transmission & Distribution*, vol. 9, no. 15, pp. 2261–2275, 2015.
- [4] W. K. Najj, H. Zeineldin, A. H. K. Alaboudy, and W. L. Woon, "A bayesian passive islanding detection method for inverter-based distributed generation using esprit," *IEEE Transactions on Power Delivery*, vol. 26, no. 4, pp. 2687–2696, 2011.
- [5] K. El-Arroudi and G. Joos, "Data mining approach to threshold settings of islanding relays in distributed generation," *IEEE Transactions on power systems*, vol. 22, no. 3, pp. 1112–1119, 2007.
- [6] Z.-L. Gaing, "Wavelet-based neural network for power disturbance recognition and classification," *IEEE transactions on power delivery*, vol. 19, no. 4, pp. 1560–1568, 2004.
- [7] N. W. A. Lidula and A. D. Rajapakse, "A pattern-recognition approach for detecting power islands using transient signals—part ii: Performance evaluation," *IEEE Transactions on Power Delivery*, vol. 27, no. 3, pp. 1071–1080, 2012.
- [8] O. N. Faqhruldin *et al.*, "A universal islanding detection technique for distributed generation using pattern recognition," *IEEE Transactions on Smart Grid*, vol. 5, no. 4, pp. 1985–1992, 2014.
- [9] A. Khamis, Y. Xu, Z. Y. Dong, and R. Zhang, "Faster detection of microgrid islanding events using an adaptive ensemble classifier," *IEEE Transactions on Smart Grid*, vol. 9, no. 3, pp. 1889–1899, 2016.
- [10] X. Liu, D. Laverty, R. Best, K. Li, D. Morrow, and S. McLoone, "Principal component analysis of wide-area phasor measurements for islanding detection—a geometric view," *IEEE Transactions on Power Delivery*, vol. 30, no. 2, pp. 976–985, 2015.
- [11] I. Zografopoulos and C. Konstantinou, "Detection of malicious attacks in autonomous cyber-physical inverter-based microgrids," *IEEE Transactions on Industrial Informatics*, 2021.
- [12] C. Li, C. Cao, Y. Cao, Y. Kuang, L. Zeng, and B. Fang, "A review of islanding detection methods for microgrid," *Renewable and Sustainable Energy Reviews*, vol. 35, pp. 211–220, 2014.
- [13] Q. Sun *et al.*, "An islanding detection method by using frequency positive feedback based on flr for single-phase microgrid," *IEEE Transactions on Smart Grid*, vol. 8, no. 4, pp. 1821–1830, 2015.
- [14] P. Gupta, R. Bhatia, and D. Jain, "Active rocof relay for islanding detection," *IEEE Transactions on Power Delivery*, vol. 32, no. 1, pp. 420–429, 2016.
- [15] M. Seyedi, S. A. Taher, B. Ganji, and J. Guerrero, "A hybrid islanding detection method based on the rates of changes in voltage and active power for the multi-inverter systems," *IEEE Transactions on Smart Grid*, vol. 12, no. 4, pp. 2800–2811, 2021.
- [16] D. G. Photovoltaics and E. Storage, "IEEE standard for interconnection and interoperability of distributed energy resources with associated electric power systems interfaces," *IEEE Std*, 2018.
- [17] S. Liu, X. Wang, and P. X. Liu, "Impact of communication delays on secondary frequency control in an islanded microgrid," *IEEE Transactions on Industrial Electronics*, vol. 62, no. 4, pp. 2021–2031, 2014.
- [18] A. Sargolzaei *et al.*, "Detection and mitigation of false data injection attacks in networked control systems," *IEEE Transactions on Industrial Informatics*, vol. 16, no. 6, pp. 4281–4292, 2020.
- [19] S. Sahoo, S. Mishra, J. C.-H. Peng, and T. Dragicevic, "A stealth cyber attack detection strategy for dc microgrids," *IEEE Transactions on Power Electronics*, 2018.
- [20] A. U. Haque, M. H. Nehrir, and P. Mandal, "A hybrid intelligent model for deterministic and quantile regression approach for probabilistic wind power forecasting," *IEEE Transactions on power systems*, vol. 29, no. 4, pp. 1663–1672, 2014.
- [21] J. Wang and J. Hu, "A robust combination approach for short-term wind speed forecasting and analysis—combination of the arima (autoregressive integrated moving average), elm (extreme learning machine), svm (support vector machine) and lssvm (least square svm) forecasts using a gpr (gaussian process regression) model," *Energy*, vol. 93, pp. 41–56, 2015.
- [22] Z. H. Zhou, "Ensemble learning," in *Machine learning*. Springer, 2021, pp. 181–210.
- [23] S. Ardabili, A. Mosavi, and A. R. Várkonyi-Kóczy, "Advances in machine learning modeling reviewing hybrid and ensemble methods," in *International Conference on Global Research and Education*. Springer, 2019, pp. 215–227.
- [24] S. Ryu, H. Choi, H. Lee, and H. Kim, "Convolutional autoencoder based feature extraction and clustering for customer load analysis," *IEEE Transactions on Power Systems*, vol. 35, no. 2, pp. 1048–1060, 2019.
- [25] G. Patsakis, D. Rajan, I. Aravena, and S. Oren, "Strong mixed-integer formulations for power system islanding and restoration," *IEEE Transactions on Power Systems*, vol. 34, no. 6, pp. 4880–4888, 2019.
- [26] M. Zhang and J. Chen, "Islanding and scheduling of power distribution systems with distributed generation," *IEEE Transactions on Power Systems*, vol. 30, no. 6, pp. 3120–3129, 2014.
- [27] P. M. Subcommittee, "IEEE reliability test system," *IEEE Transactions on power apparatus and systems*, no. 6, pp. 2047–2054, 1979.